HHS Public Access

Author manuscript

Nat Chem Biol. Author manuscript; available in PMC 2020 July 20.

Published in final edited form as:

Nat Chem Biol. 2020 February ; 16(2): 188–196. doi:10.1038/s41589-019-0449-5.

Biased modulators of NMDA receptors control channel opening and ion selectivity

Riley E. Perszyk[1], **Sharon A. Swanger**[1,2], **Chris Shelley**[1,3], **Alpa Khatri**[1], **Gabriela Fernandez-Cuervo**[4,†], **Matthew P. Epplin**[4], **Jing Zhang**[1], **Phuong Le**[1], **Pernille Bülow**[5,6], **Ethel Garnier-Amblard**[4], **Pavan Kumar Reddy Gangireddy**[4], **Gary J. Bassell**[6], **Hongjie Yuan**[1], **David S. Menaldino**[4], **Dennis C. Liotta**[4], **Lanny S. Liebeskind**[4], **Stephen F. Traynelis**[1,*]

[1]Department of Pharmacology and Chemical Biology, Emory University School of Medicine, Atlanta, GA 30322

[2]Virginia Tech Carilion Research Institute, Roanoke, VA 24016; Department of Internal Medicine, Virginia Tech Carilion School of Medicine, Roanoke, VA 24016; Department of Biomedical Sciences and Pathobiology, Virginia-Maryland School of Veterinary Medicine, Virginia Tech, Blacksburg, VA 24061

[3]Department of Biology, University of the South, Sewanee, TN 37383

[4]Department of Chemistry, Emory University, Atlanta, GA 30322

[5]Department of Physiology, Emory University, Atlanta, GA 30322

[6]Department of Cell Biology, Emory University, Atlanta, GA 30322

Abstract

Allosteric modulators of ion channels typically alter the transitions rates between conformational states without changing the properties of the open pore. We describe here a novel class of positive allosteric modulators of N-methyl D-aspartate receptors (NMDARs) that mediate a calcium-

*Correspondence to: Stephen F. Traynelis, 1510 Clifton Rd NE, Atlanta, GA, 30322, strayne@emory.edu, 404-727-0357.
†Current address: Department of Pathology, Stanford University School of Medicine, 300 Pasteur Drive, Stanford, CA

Author Contribution

The authors contributed in the following manner: conceptualization (SFT, REP, SAS), data curation and formal analysis (REP, SAS, CS, AK, GFC, HY, SFT), funding acquisition (SAS, SFT, HY, DCL, GJB), investigation (REP, SAS, CS, AK, JZ, PL, EGA, GFC, MPE, DSM, PB), development or design of methodology (REP, SAS, SFT, EGA, GFC, MPE, GJB, DSM, DCL, LSL), project administration (REP, SFT, SAS), provision of reagents, materials, and analysis tools (PKRG, EGA, GFC, PB, GJB, MPE, DSM, DCL, LSL), software (REP, SFT), supervision (SFT, LSL, DCL, GJB), verification (REP, SAS, CS, AK, GFC, MPE, DSM), visualization and writing (all authors).

Data Availability:

The data that support the findings of this study are available from the corresponding author upon reasonable request.

Code Availability:

The code that support the analysis of the findings contained in this study are available from the corresponding author upon reasonable request.

Ethics approval:

The experiments requiring primary neuronal tissue from rats and mice were conducted according to the guidelines by the Emory University Institutional Animal Care and Use Committee, and were performed in accordance with state and federal Animal Welfare Acts and the policies of the Public Health Service.

permeable component of glutamatergic synaptic transmission and play essential roles in learning, memory, cognition, as well as neurological disease. EU1622-14 increases agonist potency and channel open probability, slows receptor deactivation, in addition to decreasing both single channel conductance and calcium permeability. The unique functional selectivity of this chemical probe reveals a mechanism for enhancing NMDAR function while limiting excess calcium influx, and shows that allosteric modulators can act as biased modulators of ion channel permeation.

One Sentence Summary

A new generation of NMDA receptor modulators control both channel opening and ionic selectivity of the channel pore.

Introduction

The excitatory neurotransmitter glutamate acts on multiple glutamate receptors, including NMDARs. Activation of NMDARs following the binding of glutamate and glycine produces an inward current when neuronal depolarization reduces the voltage-dependent channel block by extracellular Mg^{2+}. These properties allow coincident pre- and post-synaptic neuronal activity to trigger synaptic plasticity, which is a cellular correlate of learning and memory[1]. Evidence from experimental, clinical, and genetic studies implicate NMDAR hypofunction in schizophrenia, intellectual disability, autism, and Alzheimer's disease. These conditions have stimulated interest in positive allosteric modulators of NMDARs as a potential therapeutic strategy for treating the associated cognitive deficits[2–7].

While NMDARs are essential for normal brain function, overactivation of NMDARs and the resulting excess calcium influx can trigger cell death[8,9], which complicates strategies to enhance NMDAR function[10,11]. One approach to enhance NMDAR function is to increase the concentration of the co-agonists glycine or D-serine with inhibitors of glycine transporter-1 or D-amino oxidase. However, this strategy has limited efficacy due to compensatory down-regulation of NMDARs that accompanies persistent activation, perhaps as a protective mechanism to avert toxicity[12]. NMDARs are tetrameric assemblies of two glycine-binding GluN1 and two glutamate-binding GluN2 subunits, of which there are four subtypes GluN2A-2D[1]. The recent development of subunit-selective NMDAR positive allosteric modulators should allow cell-type- or circuit-specific modulation due to spatially-distinct GluN2 expression, without global NMDAR overactivation[13–20]. However, while positive allosteric modulators act only when agonist is present to enhance NMDAR function, there remains a risk for overactivation at some synapses. Here we describe the development of biased allosteric modulators that differentially regulate various aspects of NMDAR signaling, such as open probability and Ca^{2+} permeability. We identified candidate molecules using a high-throughput assay[21] to screen 100,000 compounds for modulation of the NMDAR response to maximally-effective concentrations of glutamate and glycine without actions at the orthosteric site or within the channel pore. We executed a medicinal chemistry campaign around one positive allosteric modulator identified in this screen with structural determinants in a region (pre-M1) known to influence single channel conductance[22]. This class of chemical probes we show regulates both channel gating and ionic selectivity, and thus establish a new precedent in ion channel biology that could allow

the tuning of specific facets of NMDAR signaling that contribute to circuit function or are dysregulated in disease. For example, biased allosteric modulators that enhance NMDAR open probability while decreasing NMDAR permeability to Ca^{2+} could allow the enhancement of NMDAR currents while protecting neurons from calcium-induced toxicity.

Results

EU1622-1 is a pan-NMDAR positive allosteric modulator

In development of an NMDAR modulator series with unique properties, we searched for novel allosteric modulators using a fluorescence-based screen[21], and identified the thienopyrimidinone EU1622-1 (Compound **1**, Figure 1A) as a potentiator of NMDAR-mediated Ca^{2+} responses. Voltage-clamp recordings from neurons (Supplementary Figure 1) and recombinant NMDARs (Figure 1B–D) demonstrated that EU1622-1 potentiated currents produced by saturating concentrations of agonists to 1.6–2.8-fold of control, and up to 8-fold at sub-saturating agonist concentrations (Supplementary Table 1). EU1622-1 had minimal effects on AMPA receptors at 100 μM (88 ± 6.4% of control, n = 11). EU1622-1 potentiation of NMDARs expressed in human embryonic kidney (HEK) cells exhibited the typical features of modulators with an extracellular binding site, including a concentration-dependent association rate, a concentration-independent dissociation rate, and a kinetically determined K_D (22 μM) consistent with the EC_{50} value (15 μM, Figure 1D, Supplementary Table 1). EU1622-1 enhanced the potency of both glutamate and glycine by 1.7- and 2.2-fold at GluN1/GluN2B, respectively, consistent with an increase in the maximal achievable potentiation for currents activated by sub-saturating agonist concentration (Figure 1E–F, Supplementary Table 2).

NMDARs are tetrameric assemblies of GluN1 and GluN2 subunits, and the two turn pre-M1 helix within each subunit lies parallel to the membrane near the extracellular vestibule of the channel. The pre-M1 linker region is involved in opening of the pore by its connection between the agonist binding domain (ABD) and the M1 helix of the transmembrane domain (TMD), as well as its contact with the M3 helix that forms the channel gate[23–31]. Cryo-electron microscopy studies of glutamate receptors suggest that rearrangements of the ABD upon agonist binding are transduced to the TMD through the linker and pre-M1 helix, which allow for movement of the M3 helix to permit ion permeation[32,33]. The pre-M1 helix harbors structural determinants of action for both negative and positive allosteric modulators[26,30,31]. Given the role of the pre-M1 helix in gating and its proximity to the structural determinants of ion selectivity[34], we hypothesized that chemical probes binding near this region might regulate channel gating and influence ion permeation, producing unique biological consequences. To test whether EU1622-1 interacted with this key region, we utilized chimeric receptor subunits as a first-pass assessment. Deletion constructs of the GluN2B, GluN2C, or GluN2D amino terminal domain had no effect on potentiation by EU1622-1, whereas replacement of the GluN2A S1-M1 region with that from GluN2D rendered the chimeric receptors sensitive to EU1622-1 in the presence of maximal concentrations of glutamate and glycine (Supplementary Table 3). Scanning site-directed mutagenesis revealed that the pre-M1 linker/M1 helix harbored structural determinants for EU1622-1 action on GluN1/GluN2B and GluN1/GluN2D receptors (Supplementary Figure

2, 3). These data suggest that EU1622-1 is an allosteric modulator that potentiates macroscopic NMDAR responses by acting through the pre-M1/M1 region.

EU1622 induces new channel subconductance levels

Given the suggestion that EU1622-1 may interact with key gating domains, we subsequently evaluated the effects of EU1622-1 on channel properties. Interestingly, single channel analysis of EU1622-1 effects on GluN1/GluN2B channels in excised outside-out patches from HEK cells reveal a striking change in single channel conductance (Figure 2), which has not previously been reported for any modulator of ligand gated ion channels, although modulators acting at the K^+ channel selectivity filter have been described[35]. We observed a decrease in channel conductance from two conductance levels of 79 ± 1.3 pS (81%) and 64 ± 4.9 pS (19%, n = 3) in vehicle to three conductance levels of 76 ± 4.5 (20%), 63 ± 3.4 (49%), and 48 ± 0.5 pS (31%) in EU1622-1. EU1622-1 potentiation arises from increased open probability with reduced channel conductance; there is no change in the channel mean open duration (Figure 2C,D). Additionally, direct transitions between subconductance levels were observed, suggesting that EU1622-1 induces different receptor states with a different permeation pathway (Figure 2E). To confirm that EU1622-1 also reduces conductance of GluN1/GluN2B, GluN1/GluN2C, and GluN1/GluN2D receptors, we analyzed the relationship between the current amplitude and variance during NMDAR activation, also known as noise analysis[36], which contains information about the unitary average chord conductance of individual channels in the macroscopic response. EU1622-1 significantly reduced chord conductance in all diheteromeric NMDARs (Supplementary Table 4)

EU1622-14 is a more potent and efficacious PAM

To better understand this effect, we sought additional analogues within this series. We synthesized more than 80 new analogues of EU1622-1, and selected EU1622-14 (Compound **2**) as a more efficacious allosteric modulator with improved solubility over other active analogues (Supplementary Figure 4, Supplementary Table 1, Supplementary Table 5). EU1622-14 showed the same subunit selectivity (Supplementary Table 1, Figure 3) and structural determinants of action as EU1622-1 (Supplementary Table 6). Given that EU1622-1 alters agonist potency, we speculated that EU1622-14 may also impact NMDAR activation time course, which is an important determinant of synaptic function of NMDARs. Thus, we simulated synaptic activation using rapid solution exchange experiments and tested whether EU1622-14 altered the time course of NMDAR deactivation following rapid removal of glutamate, which controls the time course of glutamatergic synaptic transmission[37]. We found that the deactivation time course of recombinant NMDARs following the removal of glutamate was prolonged in the presence of EU1622-14 compared to vehicle for all subunit combinations (Figure 3A,B, Supplementary Figure 5, Supplementary Table 7), consistent with the observation that analog modulators enhance agonist potency. In some instances, potentiation of amplitude and deactivation time course approached a 10-fold increase over control. Given the effect of EU1622-1 on channel conductance, we tested whether EU1622-14 had similar actions. To screen for this effect, we used variance analysis to evaluate EU1622-14's effect on channel conductance from HEK cells expressing GluN1/GluN2A, GluN1/GluN2B, GluN1/GluN2C, or GluN1/GluN2D

(Figure 3C,D)[36]. Like EU1622-1, EU1622-14 significantly reduced the conductance in all GluN2 NMDARs, consistent with actions at all NMDAR subunit combinations (Figure 3E).

EU1622-14 reduces channel conductance in native cells

To evaluate the effects of EU1622-14 on native NMDARs, we recorded single channel currents in outside-out patches excised from cultured cortical neurons that express GluN2A and GluN2B (Figure 4)[38]. We analyzed the relative frequencies and durations of the NMDA-activated main conductance and subconductance levels in outside-out patches that contained 1 or a few channels in external solution with physiological levels of free Ca^{2+} (1.25 mM). EU1622-14 (50 μM) clearly decreased single channel chord conductance from two levels in vehicle (51 ± 0.8 pS, 88%; 42 ± 1.0 pS, 12%; n = 6) to three lower levels (44 ± 1.1 pS, 59%; 32 ± 0.5 pS, 38%; 25 ± 0.9 pS, 3%) when the same patch was treated with EU1622-14 (Figure 4A,C, Supplementary Table 8). None of these sublevels were apparent in the absence of the agonist NMDA or in the presence of 50 μM D-APV and 7-chlorokynurenate, confirming they arose from NMDARs. The observed conductance states in the presence of EU1622-14 were unique from those observed in control, suggesting that the modulator either alters the ionic selectivity of the NMDAR, or enables the NMDAR channel pore to adopt a unique set of conformations that leads to an overall reduction in ion flux. We observed direct transitions between the modulator-induced subconductance states, indicating that a single channel can occupy these distinct levels (Figure 4A). As expected from the macroscopic response of EU1622-1 in neurons (Supplementary Figure 1), the open probability of native NMDARs increased 4.4-fold in EU1622-14 ($p = 0.016$, paired t-test, Supplementary Table 8). Both drug and agonist were applied at 4–5 fold EC_{50} (Supplementary Table 1, 93–97% occupancy)[39], suggesting that the receptor shifts between these distinct conductance states when drug is bound, although it is possible that the full conductance levels are reached when the drug has dissociated from the receptor. Because extracellular Ca^{2+} can influence single channel conductance[40–42], we evaluated the effects of EU1622-14 on neuronal NMDAR chord conductance and mean channel open time in reduced Ca^{2+} (0.5 mM). We observed two conductance levels of 61 ± 1.9 (81%) and 51 ± 2.2 pS (19%) in vehicle (mean ± sem, n=4). In the presence of 50 μM EU1622-14, we observed conductance levels of 54 ± 2.0 (67%), 43 ± 2.6 (26%), and 29 ± 5.6 pS (7%) (Figure 4B,D). Thus, the reduction by EU1622-14 of conductance levels appears independent of the external Ca^{2+} concentration. The effects of the EU1622 series create a new precedent for the modulation of the ionic selectivity of ligand-gated channels.

Subconductance levels have reduced Ca^{2+} permeability

A reduction in single channel conductance must reflect a reduction in the flux of cations through the pore due either to electrical or steric effects within the permeation path. Given the distinct atomic radii and hydration energies for Na^+ and Ca^{2+}, it seems unlikely that a change in conductance will reflect equal decrements in Ca^{2+} and Na^+ permeability. Rather, we predicted that EU1622-14 changes the relative permeability of monovalent and divalent ions. We determined the relative NMDAR Ca^{2+}-monovalent permeability in HEK cells by recording the current-voltage relationship (I-V) in 0.1 mM or 10 mM Ca^{2+} (Supplementary Figure 6). We calculated the Ca^{2+} permeability relative to monovalent permeability from the reversal potential shifts using the Lewis equation (Figure 5, Supplementary Table 9)[43–46].

EU1622-14 significantly reduced the calcium permeability ratio for both GluN1/GluN2A and GluN1/GluN2B. We repeated these experiments using a different set of biionic solutions that allowed the determination of the Ca^{2+}/Cs^{+} permeability ratio in lower Ca^{2+} (0, 1.8 mM), which confirmed that 50 μM EU1622-14 reduced the relative permeability to Ca^{2+} (Supplementary Figure 7). To determine whether this was a feature in general of NMDAR positive allosteric modulators, we evaluated compound (−)-EU1180-325 (Compound **3**, compound *S*-(−)-2 in Strong et al. 2017), which potentiated the response to maximally effective glutamate and glycine in GluN1/GluN2B, GluN1/GluN2C, and GluN1/GluN2D receptors expressed in HEK cells in a similar fashion to EU1622-14[18]. We found no detectable change in unitary currents determined from variance analysis (Supplementary Table 4), and no detectable change in the permeability ratio for Ca^{2+} and Na^{+} (as determined by the biionic method, Supplementary Figure 7), despite robust enhancement of the NMDAR response (Supplementary Table 9). This is similar to the result obtained with a close analogue, CIQ, which has no effect on GluN1/GluN2D unitary current[20].

Because similar structural determinants control Ca^{2+} and Mg^{2+} permeation[44], we reasoned that any change in Ca^{2+} permeation may produce modest changes in Mg^{2+} sensitivity. We recorded I-V curves in 0.3 or 1.0 mM extracellular Mg^{2+} in the absence and presence of 50 μM EU1622-14. We found that EU1622-14 reduced the sensitivity to Mg^{2+} with no change in the reversal potential (Supplementary Figure 8). Analysis with the Woodhull equation suggests EU1622-14 increased the $K_{D,0mV}$ for Mg^{2+} (Supplementary Table 10)[47]. The reduced Ca^{2+} permeability coupled with enhanced NMDAR opening renders EU1622-14 a unique modulator that can enhance NMDAR function while limiting calcium influx and attendant toxicity.

Net modulation results in reduced relative Ca^{2+} influx

To determine the net effect of the positive allosteric modulation and reduced calcium permeability we measured the total current influx using patch-clamp recording while simultaneously imaging the change in the fluorescence of the cell-impermeant Ca^{2+}-sensitive dye Calbryte 590 (Figure 6A–C). Upon the application of NMDA in the presence of vehicle, we observed an average peak current response of 2990 ± 730 pA and the slope of the rise of the Ca^{2+}-dependent fluorescence was 8.06 [4.17, 12.0] ΔF/min (mean fitted slope [confidence interval], converted from units based on frames to minutes). In the presence of 50 μM EU1622-14, the average peak current response of 9460 ± 1240 pA and the slope of the Ca^{2+}-sensitive dye was 14.2 [8.18, 20.1] ΔF/min. The inferred net effect caused by EU1622-14 modulation in this dataset was an increase in total current 3.17 fold whereas the increase in the change in fluorescence was only 1.75 fold. To determine if EU1622-14 can alter NMDAR-mediated Ca^{2+} influx into neurons that are neither dialyzed nor under voltage clamp, we utilized fluorescent dyes to concurrently measure relative changes in the intracellular Ca^{2+} and Na^{+} during NMDAR activation in the absence and presence of EU1622-14. We loaded cultured cortical neurons with the Na^{+}-sensitive dye CoroNa Green and Ca^{2+}-sensitive dye Calbryte 590, which have non-overlapping excitation-emission spectra, allowing dual imaging during NMDAR activation. We measured the rate of change in the Na^{+}-signal and the Ca^{2+}-signal fluorescence during NMDA/glycine application in the presence of vehicle or 50 μM EU1622-14 (Figure 6D–G). NMDA treatment induced a rapid

increase in both CoroNa Green fluorescence (0.89 [0.70, 1.08] ΔF/min, which was sensitive to the open channel blocker memantine, Figure S9), and Calbryte 590 fluorescence (4.23 [2.19, 6.27] ΔF/min). In the presence of EU1622-14, the rate of change of the NMDA-induced in CoroNa Green fluorescence (1.70 [1.06, 2.35] ΔF/min) was greater than in vehicle, and NMDA-induced increase in Calbryte 590 fluorescence (6.17 [1.24, 11.1] ΔF/min) was modestly higher than vehicle. That is, EU1622-14 accelerated the rate of rise in the CoroNa Green signal (Na^+ sensitive, EU1622-14/vehicle ratio 1.91) to a greater extent than the increase in the Calbryte 590 signal (Ca^{2+} sensitive, EU1622-14/vehicle ratio 1.46), a result that is consistent with the patch-clamp/imaging experiment. Subsequent application of A23187 (10 μM) was used to show that the calcium signal was not saturated during agonist stimulation in these experiments (Supplementary Figure 9B). Additionally, the increase in Calbryte 590 AM fluorescence due to A23187 ionophore alone was unaffected by the presence of EU1622-14, which suggests that the reduction in calcium permeability is not due to a non-specific interaction of EU1622-14 with free-Ca^{2+} or due to modification of Ca^{2+} handling. We also evaluated the NMDAR PAM (−)-EU1180-325 in these same assays, and observed similar increases in Na^+ or Ca^{2+} signals, suggesting that NMDARs potentiated by (−)-EU1180-325 do not exhibit reduced relative Ca^{2+} influx (Supplementary Figure 10). Taken together, these results indicate that the net effect of EU1622-14 modulation causes a robust increase in the Na^+ influx during NMDAR activation associated with a modest increase in Ca^{2+} influx.

Discussion

NMDARs play critical roles in the brain, and thus it is important to understand their function at an atomic level. In addition, NMDARs are an important therapeutic target, given that NMDAR hypoactivity is involved in the pathophysiology of several neurological conditions, while overactivation of NMDARs is associated with excitotoxicity and cell death following acute injury. These opposing consequences of NMDAR dysregulation present a problem for developing therapies to treat diseases involving NMDAR hypofunction, as persistent enhancement of NMDAR activation is not a viable therapeutic approach. The major advance provided by this work is the discovery of a chemical series of allosteric modulators that have structural determinants in a key gating region and enhance function through an increase in both agonist potency and open probability, but with decreased single channel conductance and lower calcium permeability. The biological effect revealed through these new chemical probes expands the repertoire of strategies for modulating ion channel function by demonstrating that functional selectivity can be achieved for all aspects of ion channel function, including ion permeation properties. That is, our data suggests that it may be possible to develop therapeutics that are selective for a particular aspect of NMDAR signaling, such as the Ca^{2+}/Na^+ permeability ratio. This form of biased signaling modulation specifically of ion permeability has not previously been established for ligand-gated ion channels, and EU1622 modulators show that it is possible for small molecules to produce allosteric modulation of agonist potency, agonist efficacy, and calcium permeability. Reduced Ca^{2+} permeability in particular could circumvent potential limitations of NMDAR potentiation by limiting excess calcium influx and excitotoxicity in neurons.

We can only speculate, at this time, as to what mechanistically brings about this reduced calcium permeability. However, there are at least three possibilities. First, these modulators might enable current flow when the receptor does not normally conduct ions, perhaps when only a subset of the subunits are in the active state or when the receptor is in a desensitized state[25,48]. Second, EU1622 binding could influence the interaction of Ca^{2+} with the DRPEER motif, which has been shown to alter ion flow through the pore[34]. The presence of extracellular Ca^{2+} increases the prevalence of subconductance levels, so it is plausible that the allosteric modulator mimics this action[41]. Third, allosteric modulators may directly alter the geometry of the permeation pathway, which could alter ion flux and/or dehydration energies for permeant ions. Studies in K^+ channels have shown that different conductance states can have different ionic selectivity[49]. While it is possible that in the presence of EU1622-14 Ca^{2+} becomes a weak channel blocker, this should impact all channel openings, and thus cannot explain the appearance of new sublevels. Determination of the mechanism of action would advance our understanding of how these channels operate, and catalyze the development of compounds that are biased modulators that tune up and down different functional modalities. Elucidating the mechanism of action of this biased allosteric modulation has the potential to reveal new insight into ion channel function and modulation.

Because of the critical actions of NMDARs in the brain, effective and well-tolerated therapeutic strategies may need to control one particular facet of NMDAR function that would be beneficial in a particular disease state. For example, development of a modulator that selectively reduces Ca^{2+} permeation through NMDARs while having minimal effects on other NMDAR properties such as agonist potency and open probability may be possible and might have neuroprotective effects in ischemic or neurodegenerative conditions without engaging known on-target side effects of NMDAR antagonism[50]. More broadly, this conceptual advance implies that small molecules could be developed to modulate ion selectivity of other ligand-gated ion channels, which could be useful not only in neurological diseases, but also in cardiac, epithelial, and inflammatory tissues where diseases are associated with aberrant Ca^{2+} influx as well.

In summary, we use chemistry to probe the mechanism of a class of allosteric modulators not previously described in literature that can decrease conductance and reduce calcium permeability, while increasing agonist potency, deactivation time course, and open probability. This form of biased signaling modulation (i.e. altering permeation properties) expands the repertoire of strategies for controlling ion channel function. This work establishes a precedent and raises the possibility of identifying compounds that simultaneously increase and decrease the contributions of specific aspects of ionotropic signaling of NMDARs. Such compounds could have unique effects on neuronal function, and be optimized through medicinal chemistry for therapeutic gain.

Online Methods

Molecular Biology

Recombinant receptors were expressed from cDNAs encoding rat GluN1-1a (hereafter GluN1, U08261), GluN2A (D13211), GluN2B (U11419), GluN2C (M91563), and GluN2D (L31611). Site-directed mutagenesis was used to introduce amino acid substitutions

according the QuikChange protocol (Agilent, Santa Clara, CA). All mutant cDNAs were subjected to Sanger sequencing to verify the mutation.

Two-electrode voltage-clamp recordings in *Xenopus* oocytes

cRNA was transcribed *in vitro* from plasmids containing NMDAR cDNAs. *Xenopus laevis* stage VI oocytes (Ecocyte Biosciences) were injected with 5–10 ng cRNA and stored at 15°C in media containing (in mM) 88 NaCl, 2.4 $NaHCO_3$, 1 KCl, 0.33 $Ca(NO_3)_2$, 0.41 $CaCl_2$, 0.82 $MgSO_4$, 5 HEPES, 1 U/mL penicillin, 0.1 mg/mL gentamicin sulfate, and 1 μg/mL streptomycin (pH 7.4, adjusted with NaOH). Two to seven days after injection, two-electrode voltage-clamp recordings were performed at room temperature (23°C) in extracellular solution containing (in mM) 90 NaCl, 1 KCl, 10 HEPES, 0.5 $BaCl_2$, and 0.01 EDTA (pH 7.4, adjusted with NaOH). NMDAR current responses from oocytes were recorded at a holding potential of −40 mV; only oocyte recordings with a maximal response amplitude greater than 50 nA were analyzed. Concentration–response curves for EU1622 compounds were generated by applying glutamate and glycine at the concentrations stated in figure legends or text, followed by variable concentrations of test compound up to 100 μM. Test compounds were prepared as 20 mM stock solutions in DMSO, and diluted to the final concentration in recording solution. DMSO content was 0.05–0.5% (v/v). EU1622-14 had a solubility determined by nephelometry to be in excess of 100 μM, considerably higher than compound **10** which precipitated at high concentrations. For some experiments 10 mM 2-(hydroxypropyl)-β-cyclodextrin was added.

Concentration-response data was analyzed using OriginPro 9.0. For potentiation concentration-response curves, the response evoked by test compounds was given as a percentage of the initial response to glutamate and glycine alone. Data for individual cells were fitted with the Hill equation:

$$Response(\%) = (Maximal\ Potentiation - 100)/(1 + (EC_{50}/[P])^{H}) + 100 \quad (1)$$

where *Maximal Potentiation* is the maximum response predicted for saturating concentrations of the positive allosteric modulator, EC_{50} is the concentration that produces a half-maximal potentiation, [P] is the concentration of positive allosteric modulator, and H is the Hill slope. For agonist concentration-response curves, the data for individual cells were fit with:

$$Response(\%) = Maximal\ Response/(1 + (EC_{50}/[agonist])^{H}) \quad (2)$$

where EC_{50} is the concentration of *agonist* that produces half of the *Maximal Response* and H is the Hill slope. Fitted EC_{50} values from individual cells were used to calculate the mean EC_{50} values. The log(EC_{50}) was used to determine the lower and upper confidence levels (LCL,UCL) of the 95% confidence interval (CI), which were then transformed back to concentration and reported with the mean EC_{50} value. For the graphical representation, the data were normalized to the current response to agonist alone, averaged across all cells, and fitted with the Hill equation.

HEK cell and neuronal cultures

HEK-293 cells (CRL 1573, ATCC; hereafter HEK cells) were cultured in DMEM (Cat # 10566016, ThermoFisher Scientific) supplemented with 10% fetal bovine serum (FBS), 10 U/ml penicillin, and 10 μg/ml streptomycin and maintained at 5% CO_2 in a 37°C incubator. HEK cells were plated on poly-D-Lysine coated glass coverslips (0.1 mg/mL, Warner Instruments) 48 hr prior to patch clamp recording. Calcium phosphate transfection was used to transiently transfect HEK cells in a 24-well plate with 500 ng of DNA at a ratio of 1:1:5 (GluN1:GluN2A:GFP) or 1:1:1 (GluN1:GluN2B:GFP), and four hours after transfection, NMDAR antagonists D,L-2amino-5-phosphonovalerate (200 μM, DL-APV) and 7-chlorokynurenic acid (200 μM) were added to the culture medium to decrease the cytotoxic effect of NMDAR expression.

Timed pregnant C57BL/6J mice were obtained from Charles River, and primary cortical neurons were cultured from the embryos at E17.5 or primary hippocampal neurons cultured from post-natal pups at P0-2. These procedures were approved by the Emory University Institutional Animal Care and Use Committee, and were performed in accordance with state and federal Animal Welfare Acts and the policies of the Public Health Service. Cortices or hippocampi were dissected from the embryos, trypsinized (0.25%) at 37°C, rinsed with warm Hank's balanced salt solution (HBSS) containing 10 mM HEPES (HBSS/HEPES), and dissociated in MEM (Cellgro) containing 10% FBS (MEM/FBS). The neurons were washed with warm HBSS/HEPES immediately following the dissection. Cells were plated in MEM/FBS on coverslips coated with 0.5–1 mg/ml poly-L-lysine). Two hours after plating, the neurons were cultured with conditioned Neurobasal medium (Life Technologies) with 1× Glutamax (Life Technologies) and 1× B-27 (Life Technologies). Media was previously conditioned by incubation with secondary mouse glia for 24 hrs. Neurons were cultured at 5% CO_2 and 37°C with 50% of the media exchanged every 3–4 days until used 5–10 days after plating.

Whole-cell voltage-clamp recordings

The current response time course was determined from whole cell patch recording of transiently transfected HEK cells or primary cultured hippocampal neurons. Whole-cell voltage-clamp recordings were performed with thin-walled borosilicate glass electrodes (3–4 MΩ, TW150F-4, World Precision Instruments) filled with solution containing (in mM) 110 Cs-gluconate, 30 CsCl, 5 HEPES, 4 NaCl, 0.5 $CaCl_2$, 2 $MgCl_2$, 5 BAPTA, 2 NaATP, 0.3 NaGTP (pH 7.35). The extracellular recording solution contained (in mM) 150 NaCl, 10 HEPES, 3 KCl, 0.5 $CaCl_2$, and 0.01 EDTA (pH 7.4). Cells were held under voltage clamp at −60 to −80 mV (not corrected for the junction potential of +12 mV) at 23°C. Rapid solution exchange was performed by lifting HEK cells from the coverslip into the solution flowing from a two-barrel theta tube that was rapidly translated using a piezoelectric manipulator (Burleigh, Siskiyou). Solution exchange around an open tip (10–90% rise time) was < 1 ms. Whole cell recordings from primary cultured hippocampal neurons were performed in the presence of 1 μM TTX, NMDAR responses were elicited by application of 100 μM NMDA and 3 μM glycine. Currents were recorded using an Axopatch 200B (Molecular Devices), filtered at 2 kHz (−3 dB), and digitized at 20 kHz.

The time course for onset and recovery of potentiation with test compounds were analyzed by fitting a single exponential function to the data. NMDAR deactivation time courses following rapid glutamate removal were fitted by a two-component exponential function and the time constants and relative amplitude determined for the fast and slow components, according to

$$Response = Amp_{\mathrm{FAST}}\exp\left(-time/\tau_{\mathrm{FAST}}\right) + Amp_{\mathrm{SLOW}}\exp\left(-time/\tau_{\mathrm{SLOW}}\right). \quad (3)$$

τ_{FAST} is the fast deactivation time constant, τ_{SLOW} is the slow deactivation time constant, Amp_{FAST} is the current amplitude of the fast deactivation component, and Amp_{SLOW} is the current amplitude of the slow deactivation component. The weighted deactivation time constant (τ_{W}) was calculated using the following equation:

$$\begin{aligned}\tau_{\mathrm{W}} = &\left[Amp_{\mathrm{FAST}}/(Amp_{\mathrm{FAST}} + Amp_{\mathrm{SLOW}})\right]\tau_{\mathrm{FAST}} \\ &+ \left[Amp_{\mathrm{SLOW}}/(Amp_{\mathrm{FAST}} + Amp_{\mathrm{SLOW}})\right]\tau_{\mathrm{SLOW}}.\end{aligned} \quad (4)$$

Variance analysis[6] was performed on current responses to slow application of 1–10 μM glutamate plus 30 μM glycine supplemented with vehicle or positive modulator at a holding potential of −60 mV. Agonist exchange proceeded slowly over 20–60 seconds, and both the rising and falling phases of the current response were analyzed, unless there were artifacts present. The current was divided into 30, 50, or 100 equal time increments, and the mean current found for each time period as well as the variance of the current. The plot of variance *vs.* current was fitted by the equation

$$Variance = i\,I - I^2/N \quad (5)$$

where i is the weighted mean unitary current, I is the macroscopic current amplitude, and N is the number of channels. The weighted mean unitary current is related to the unitary currents i_j for multiple j subconductance levels each with a relative probability of p_j by

$$Weighted\ mean\ unitary\ current = \Sigma_j\, i_j^{\,2}\, p_j/\Sigma_j i_j p_j. \quad (6)$$

Chord conductance γ was determined assuming a reversal potential of 0 mV.

Single channel recording

Patch pipettes were pulled from thick-walled borosilicate glass pipettes (Warner Instruments, GFC-150) to give resistances of 8–12 MΩ and their tips fire-polished and shanks coated with Sylgard elastomer (Sigma-Aldrich; St. Louis, MO). The external bath solution is given in Supplementary Table 11, and contained (in mM), 150 NaCl, 3 KCl, 11 glucose, 10 HEPES, 0.01 EDTA, 0.5 or 1.25 $CaCl_2$ (pH 7.4). The internal solution contained (in mM), 110 D-gluconate, 110 CsOH, 30 CsCl, 5 BAPTA, 5 HEPES, 4 NaCl, 2 $MgCl_2$, 2 Na-ATP, 0.5 $CaCl_2$, 0.3 Na-GTP (pH 7.35, Supplementary Table 11). Outside-out patches were excised from cortical neurons or cultured HEK cells transiently transfected with cDNA encoding NMDA receptor subunits. Patches were held under voltage clamp at −80 mV using a Warner Patch Clamp PC-505A amplifier (Warner Instruments; Hampden, CT). Signals were filtered

at 10 kHz and digitized online at 40 kHz using a USB-621 M series digitizer (National Instruments; Austin, TX) and WinEDR, part of the Strathclyde Electrophysiology Software suite (http://spider.science.strath.ac.uk/sipbs/software_ses.htm). Test solutions were applied using a gravity-fed theta tube and consisted of external bath solution. Neuronal NMDARs were activated by 100 μM glycine, 500 μM NMDA, and DMSO, or by 100 μM glycine, 500 μM NMDA, and 50 μM EU1622-14 in DMSO. All recordings were made at room temperature (23°C). NMDAR currents in outside-out patches from HEK cells were activated by 0.1 mM glutamate and 50 μM glycine plus either DMSO vehicle or with 30–50 μM EU1622-1 in DMSO. The final DMSO was 0.25% in drug and vehicle solutions.

Single Channel Analysis

Acquired data were converted to pClamp (Molecular Devices; San Jose, CA) readable abf format files for visual inspection and digitally low pass filtered at 1 or 3 kHz (−3 dB). Single channel event amplitudes and durations from outside-out patches were measured using time course fitting implemented in the SCAN program (http://www.ucl.ac.uk/Pharmacology/dcpr95.html) from data filtered at 1 kHz. The idealization and fitting of single channel recordings were performed blinded. The event transitions were fitted with a convolved filtered step-response function using a least-square criterion[51]. Analysis of event amplitudes were performed using a resolution of 2.5 filter rise-times. Amplitude histograms were fitted with one, two or three Gaussian components using maximum likelihood; currents smaller than −1 pA were omitted. The product of the number of channels (assumed to be constant during the recording period) and open probability was determined by subtracting the baseline current from each outside-out patch recording, finding the average current across the recording, and dividing this by the weighted mean unitary current amplitude for the condition.

Measurement of Ca^{2+} permeability and voltage-dependent Mg^{2+} block

The ratio of Ca^{2+} permeability to monovalent permeability was determined from the shifts in the reversal potential in solutions that contained different concentrations of permeant cations. All analyses of Ca^{2+} permeability were performed blinded. We first determined the NMDAR reversal potential in a solution that contained physiological level of Ca^{2+} (1.8 mM $CaCl_2$), lacked permeant monovalent inorganic cations, and instead contained N-methyl-D-glucamine (140 mM) and 10 mM HEPES (adjusted to pH 7.2 by adding HCl). The reversal potential in this solution was compared to that determined in a solution that contained 140 mM CsCl and 10 mM HEPES, adjusted to pH 7.2 with CsOH[45,46]. The pipette was initially placed in our standard recording solution that contained (in mM) 150 NaCl, 3 KCl, 1 $CaCl_2$, 10 HEPES (adjusted to pH 7.2 with NaOH). The reference ground communicated with this solution through a 3 M KCl agar bridge, which was replaced multiple times during each recording day. The internal pipette solution contained (in mM) 125 CsCl, 10 HEPES, 10 EGTA, adjusted to pH 7.2 with CsOH. The liquid junction potential at the tip (see Supplementary Figure 11A, JP_{LIQ1}) was calculated to be +6.6 mV (pClamp)[43,52], and the amplifier was set to balance this potential as well as any potential at the 3M KCl reference ground (the latter which does not change throughout the experiment). Upon achieving a whole cell recording with the patch pipette, the liquid junction potential is eliminated, and the amplifier now has a command voltage of −6.6 mV due to zero current adjustment

(Supplementary Figure 11B). We then moved the cell into a small 100 micrometer diameter laminar flow stream of the CsCl-HEPES solution, which provided less than 0.1% of the flow rate of the background, and thus did not create any appreciable liquid junction potential at the 3 M KCl reference electrode. There was, however, a liquid junction potential that developed at the interface of this stream near the cell and the background wash near the reference (JP_{LIQ2}) that was −5.2 mV (Supplementary Figure 11C). In the absence of agonist, we applied an incremental voltage step protocol, which started by changing the holding potential of the cell from the resting level (−60 mV) to +45 mV, and then incrementally stepped to −60, −80 or −100 mV in 2 s duration 5 mV steps (or a reverse voltage step). The voltage was not corrected for the junction potential JP_{LIQ1}. The current response was filtered at 5 kHz (8 pole Bessel, −3 dB) and digitized at 10 kHz. We subsequently activated the receptor with a maximally-effective concentration of glutamate (100 μM) and glycine (30 μM), allowed the desensitizing response to reach a steady-state plateau, and then re-applied the voltage step protocol a second time. The current-voltage relationship was determined from the mean response of the agonist-activated current – baseline current during the final 0.5 s of each voltage step. We subsequently moved the cell into a second small diameter stream of solution (100 μm in diameter) that contained Ca^{2+}/NMDG and repeated the voltage step protocol in the absence and presence of glutamate and glycine. This second solution near the cell also has a liquid junction potential of +5.0 mV (Supplementary Figure 11D). We omitted recordings from cells for which the leak current in the absence of glutamate was greater than 75% (low calcium) or 100% (high calcium) of the response in glutamate. The current-voltage curves were fitted by a 4^{th} order polynomial least-square minimization function, and the reversal potential (V_{rev}) determined by finding the root of the curve. The reversal potentials were then corrected by subtracting the above calculated junction potentials (JP_{LIQ1} and JP_{LIQ2}, or JP_{LIQ1} and JP_{LIQ3}) referenced to the pipette (See Supplementary Figure 11 legend)[52]. All junction potentials and solution compositions are given in Supplementary Tables 11–12 (Referred to as “Biionic”).

The difference in the corrected reversal potentials (ΔV_{rev}) for Ca^{2+}- and Cs^{+}-containing solutions and the corrected Ca^{2+} reversal potential were used to determine the permeability ratio of Ca^{2+} to Cs^{+} using a modified version of the Lewis equation[43], as shown below.

$$V_{\mathrm{rev,\,Ca}} - V_{\mathrm{rev,\,Cs}} = \Delta V_{\mathrm{rev}} = \frac{RT}{F}\ln\frac{4\frac{P_{\mathrm{Ca}}}{P_{\mathrm{Cs}}}\left[\mathrm{Ca}^{2+}\right]_o}{\left[\mathrm{Cs}^{+}\right]_o\left[1+\exp\left(\frac{V_{\mathrm{rev,\,Ca}}}{RT/F}\right)\right]} \tag{7}$$

$$\frac{P_{\mathrm{Ca}}}{P_{\mathrm{Cs}}} = \frac{\exp\left(\Delta V_{\mathrm{rev}}\frac{F}{RT}\right)\left[\mathrm{Cs}^{+}\right]_o\left[1+\exp\left(\frac{V_{\mathrm{rev,\,Ca}}}{RT/F}\right)\right]}{4\left[\mathrm{Ca}^{2+}\right]_o} \tag{8}$$

We also used a different set of solutions to determine the ratio of permeability of the channel for Ca^{2+} to the permeability for Na^{+} as described by[44]. These solutions contained a constant monovalent ion concentration and instead altered the external Ca^{2+} concentration; the

pipette was filled with a KCl-based solution. We assumed that the relative permeabilities of K^+ and Na^+ are the same[44,53]. The arrangement of this experiment was identical to that described above (see Supplementary Figure 11), with the solutions summarized in Supplementary Tables 11–12 (described by the phrase “High monovalent”). The current-voltage curve was established using the same protocol as before, and the reversal potential determined from a fourth order polynomial function fitted to the I-V curve. Only GluN1/GluN2A current responses less than 3000 pA were analyzed; we omitted recordings from cells for which the leak current in the absence of glutamate was greater than 40% (low calcium) or 175% (high calcium) of the response in glutamate. The reversal potentials were used to determine the ratio of the permeability of the channel to Ca^{2+} and to Na^+ from modified versions of the Lewis equation, as described below:

$$V_{\text{rev, Ca}} - V_{\text{rev, Na}} = \Delta V_{\text{rev}} = \frac{RT}{F}\ln\left(1 + \frac{4\frac{P_{\text{Ca}}}{P_{\text{Na}}}\left[\text{Ca}^{2+}\right]_o}{\left[\text{Na}^+\right]_o\left[1 + \exp\left(\frac{V_{\text{rev, Ca}}}{RT/F}\right)\right]}\right) \tag{9}$$

$$\frac{P_{\text{Ca}}}{P_{\text{Na}}} = \frac{\left[\exp\left(\Delta V_{rev}\frac{F}{RT}\right) - 1\right]\left[\text{Na}^+\right]_o\left[1 + \exp\left(\frac{V_{\text{rev, Ca}}}{RT/F}\right)\right]}{4\left[\text{Ca}^{2+}\right]_o} \tag{10}$$

Voltage-dependent Mg^{2+} block was assessed using whole cell recordings from HEK cells transiently transfected with GluN1/GluN2A/GFP or GluN1/GluN2B/GFP, as described above. Whole cell current recordings utilized the “whole cell current” internal and external solutions described in Supplementary Table 11. Holding potential was −60 mV, which was varied before and during agonist application (as described above from +40 to −80 mV in 5 mV steps) and not corrected for the +11 mV liquid junction potential in Mg^{2+}-containing solutions. The agonist–evoked current was obtained by subtracting the baseline response, and the current-voltage curve fitted by the Woodhull equation[47] modified to treat the reversal potential as a variable:

$$I = \frac{Amp\left(V_m - V_{rev}\right)}{1 + \left(\frac{\left[\text{Mg}^{2+}\right]}{K_{D,\,0mV}\exp\left(V_m z\delta / 25.693\right)}\right)} \tag{11}$$

The amplitude (*Amp*) was varied to take into account potentiation of GluN2B by extracellular Mg^{2+} [54], V_m was the holding potential, V_{rev} was the reversal potential, $K_{D,0\,mV}$ was the Mg^{2+} affinity at 0 mV for its site in the pore, and $z\delta$ the product of Mg^{2+} charge and the distance through the electric field at which the binding site resides. Extracellular Mg^{2+} was either 0.3 or 1 mM.

Calcium and sodium imaging

To reduce baseline neural activity in cortical neuron cultures, 1 μM tetrodotoxin (TTX), 200 μM APV, and 200 μM 7-chlorokyneurenic acid (7-CKA) were added to the culture media for 30 min. For dye loading, the media was removed, and neurons were incubated in dye loading buffer containing (in mM) 150 NaCl, 10 HEPES, 1 KCl, 10 glucose, 0.001 TTX, 0.2 APV, and 0.2 7-CKA with 0.5 % pluronic acid, 2.5 μg/ml CoronoGreen AM Na^+-sensitive dye (Life Technologies), and 2.5 μg/ml Calbryte 590 AM Ca^{2+}-sensitive dye (AAT Bioquest) for 30 min at 37 °C. The coverslip was transferred to an imaging chamber with imaging buffer containing (in mM) 150 NaCl, 10 HEPES, 1 KCl, 10 glucose, 0.001 tetrodotoxin (TTX), 0.002 APV, and 0.002 7-CKA, and neurons were imaged within 5 min of removal from the dye loading buffer. Vehicle (0.1 % DMSO) or EU1622-14 (50 μM) were pre-applied for 1 min in imaging buffer with sub-saturating concentrations of the competitive antagonists APV and 7-CKA to minimize NMDAR activation prior to agonist application and allow rapid dissociation upon agonist application. Then, 500 μM NMDA and 100 μM glycine were applied to activate NMDARs in the presence of vehicle or drug for 30 s in imaging buffer without APV and 7-CKA. Images were acquired with an inverted Olympus IX51 microscope equipped with a disk spinning unit, 20*X* objective, and an ORCA-ER CCD camera (Hamamatsu) controlled using MicroManager softwaree (https://micro-manager.org/). Images were acquired every 2 s (alternating between dyes) using the following emission, excitation, and dichroic filter sets for Corona Green AM and Calbryte 590 AM, respectively: 470/40, 525/50, 495 nm and 545/25, 605/70, 565 nm.

For the patch-clamp imaging experiments, cell-impermeant Calbryte 590 potassium salt was loaded (5 μg/ml) into an internal solution contained (in mM), 95 D-gluconate, 95 CsOH, 5 CsCl, 40 HEPES, 8 NaCl, 5 $MgCl_2$, 2 Na-ATP, 0.3 Na-GTP, 1 QX-314-Cl, 2 TEA-Cl (pH 7.35). The base external solution was the same as the imaging buffer but also containing 0.01 NBQX, and 0.01 bicuculline. Prior to the initiation of the experiment, five minutes was allowed for the dye to reach equilibrium after achieving the whole cell conformation. Images were acquired every 1 s. The cells were held at −60 mV for the duration of the experiment, *post hoc* access resistance filtering compensation was applied to the current recordings[55].

Within each experiment, samples from all groups were acquired in the same imaging session with identical acquisition settings. ImageJ was used for image analysis and presentation, and the experimenter was blinded to the treatment group during image analysis. Mean fluorescence intensity was measured in neuron somas, and then background subtracted using the mean fluorescence intensity of non-cellular region from the same imaging field. For presentation, the intensity settings for each channel are the same across all images at a given magnification. Data are reported as the change in fluorescence intensity ($\Delta F = F_t - F_0$) relative to the fluorescence intensity at the start of the experiment (F_0). The slopes were calculated by finding the point of maximum slope during the agonist induced rise in fluorescence intensity, then taking the average slope of the 5 (dual imaging experiments) or 11 (patch imaging experiments) data points centered on that point. The slopes from all neurons in a given field on each coverslip were averaged and the result considered one experiment.

Statistical Analysis

Prospective power analyses were performed using GPower 3.1 (http://www.psychologie.hhu.de/arbeitsgruppen/allgemeine-psychologie-und-arbeitspsychologie/gpower.html) to determine sample sizes necessary for detecting large effects (0.8–1.0) at a power of 0.80 with appropriate planned statistical tests. OriginPro 9.0 or GraphPad 5.0 were used for statistical analyses and graph preparation. Data were tested for normality with the Kolmogorov-Smirnov test, and for homogeneity of variances with Levene's test. Group comparisons were made using a t-test (paired or unpaired, as necessary) or ANOVA and post hoc tests as indicated and using two-sided assumptions. The alpha level was set at 0.05 for all experiments and corrected for multiple pairwise comparisons and familywise error rate as stated in the figure or table legends. Data were presented as the mean ± s.e.m. EC_{50} values were reported as the mean EC_{50} with LCL, UCL of the 95% CI determined from the log EC_{50} values, and comparisons were done by F tests using the logEC_{50} values.

Supplementary Material

Refer to Web version on PubMed Central for supplementary material.

Acknowledgments

The authors thank Kevin Ogden for help with analytical software development. This work was supported by the NINDS (NS065371, SFT), NICHD (HD082373, HY), NIMH (MH109026, GB), Citizens United for Research in Epilepsy (SAS) and the Emory University Research Committee (SAS).

Potential Conflict of Interests:

Several authors have competing interests; SFT is a consultant for Janssen Pharmaceuticals Inc., is PI on a research grants from Janssen and Allergan to Emory University School of Medicine, is a member of the SAB for Sage Therapeutics, is co-founder of NeurOp Inc, and receives royalties for software. DCL is a member of the Board of Directors for NeurOp Inc. DCL, DSM, EGA, GFC, PKRG, LSL, MPE, SFT are co-inventors on Emory-owned Intellectual Property that includes allosteric modulators of NMDA receptor function. HY is PI on a research grant from Sage Therapeutics to Emory University School of Medicine.

References and Notes

1. Traynelis SF et al. Glutamate receptor ion channels: structure, regulation, and function. Pharmacol Rev 62, 405–496, doi:10.1124/pr.109.002451 (2010). [PubMed: 20716669]
2. Coyle JT, Tsai G & Goff D Converging evidence of NMDA receptor hypofunction in the pathophysiology of schizophrenia. Ann N Y Acad Sci 1003, 318–327 (2003). [PubMed: 14684455]
3. Heresco-Levy U, Javitt DC, Ermilov M, Silipo G & Shimoni J Double-blind, placebo-controlled, crossover trial of D-cycloserine adjuvant therapy for treatment-resistant schizophrenia. Int J Neuropsychopharmacol 1, 131–135, doi:10.1017/S1461145798001242 (1998). [PubMed: 11281957]
4. Hu C, Chen W, Myers SJ, Yuan H & Traynelis SF Human GRIN2B variants in neurodevelopmental disorders. J Pharmacol Sci 132, 115–121, doi:10.1016/j.jphs.2016.10.002 (2016). [PubMed: 27818011]
5. Ingram DK et al. New pharmacological strategies for cognitive enhancement using a rat model of age-related memory impairment. Ann N Y Acad Sci 717, 16–32 (1994). [PubMed: 8030831]
6. Javitt DC Management of negative symptoms of schizophrenia. Curr Psychiatry Rep 3, 413–417 (2001). [PubMed: 11559479]
7. Yuan H, Low CM, Moody OA, Jenkins A & Traynelis SF Ionotropic GABA and Glutamate Receptor Mutations and Human Neurologic Diseases. Mol Pharmacol 88, 203–217, doi:10.1124/mol.115.097998 (2015). [PubMed: 25904555]

8. Choi DW Excitotoxic cell death. Journal of Neurobiology 23, 1261–1276, doi:10.1002/neu.480230915 (1992). [PubMed: 1361523]
9. Parsons MP & Raymond LA Extrasynaptic NMDA receptor involvement in central nervous system disorders. Neuron 82, 279–293, doi:10.1016/j.neuron.2014.03.030 (2014). [PubMed: 24742457]
10. Gonzalez J et al. NMDARs in neurological diseases: a potential therapeutic target. Int J Neurosci 125, 315–327, doi:10.3109/00207454.2014.940941 (2015). [PubMed: 25051426]
11. Collingridge GL et al. The NMDA receptor as a target for cognitive enhancement. Neuropharmacology 64, 13–26, doi:10.1016/j.neuropharm.2012.06.051 (2013). [PubMed: 22796429]
12. Schade S & Paulus W D-Cycloserine in Neuropsychiatric Diseases: A Systematic Review. Int J Neuropsychopharmacol 19, doi:10.1093/ijnp/pyv102 (2016).
13. Chopra DA et al. A single-channel mechanism for pharmacological potentiation of GluN1/GluN2A NMDA receptors. Sci Rep 7, 6933, doi:10.1038/s41598-017-07292-8 (2017). [PubMed: 28761055]
14. Hackos DH et al. Positive Allosteric Modulators of GluN2A-Containing NMDARs with Distinct Modes of Action and Impacts on Circuit Function. Neuron 89, 983–999, doi:10.1016/j.neuron.2016.01.016 (2016). [PubMed: 26875626]
15. Khatri A et al. Structural determinants and mechanism of action of a GluN2C-selective NMDA receptor positive allosteric modulator. Mol Pharmacol 86, 548–560, doi:10.1124/mol.114.094516 (2014). [PubMed: 25205677]
16. Perszyk RE et al. GluN2D-Containing N-methyl-d-Aspartate Receptors Mediate Synaptic Transmission in Hippocampal Interneurons and Regulate Interneuron Activity. Mol Pharmacol 90, 689–702, doi:10.1124/mol.116.105130 (2016). [PubMed: 27625038]
17. Sapkota K et al. Mechanism and properties of positive allosteric modulation of N-methyl-d-aspartate receptors by 6-alkyl 2-naphthoic acid derivatives. Neuropharmacology 125, 64–79, doi:10.1016/j.neuropharm.2017.07.007 (2017). [PubMed: 28709671]
18. Strong KL et al. The Structure-Activity Relationship of a Tetrahydroisoquinoline Class of N-Methyl-d-Aspartate Receptor Modulators that Potentiates GluN2B-Containing N-Methyl-d-Aspartate Receptors. J Med Chem 60, 5556–5585, doi:10.1021/acs.jmedchem.7b00239 (2017). [PubMed: 28586221]
19. Wang TM et al. A novel NMDA receptor positive allosteric modulator that acts via the transmembrane domain. Neuropharmacology 121, 204–218, doi:10.1016/j.neuropharm.2017.04.041 (2017). [PubMed: 28457974]
20. Mullasseril P et al. A subunit-selective potentiator of NR2C- and NR2D-containing NMDA receptors. Nat Commun 1, 90, doi:10.1038/ncomms1085 [pii] (2010). [PubMed: 20981015]
21. Hansen KB et al. Implementation of a fluorescence-based screening assay identifies histamine H3 receptor antagonists clobenpropit and iodophenpropit as subunit-selective N-methyl-D-aspartate receptor antagonists. J Pharmacol Exp Ther 333, 650–662, doi:10.1124/jpet.110.166256 (2010). [PubMed: 20197375]
22. Ogden KK et al. Molecular Mechanism of Disease-Associated Mutations in the Pre-M1 Helix of NMDA Receptors and Potential Rescue Pharmacology. PLOS Genetics 13, e1006536, doi:10.1371/journal.pgen.1006536 (2017). [PubMed: 28095420]
23. Karakas E & Furukawa H Crystal structure of a heterotetrameric NMDA receptor ion channel. Science 344, 992–997, doi:10.1126/science.1251915 (2014). [PubMed: 24876489]
24. Lee CH et al. NMDA receptor structures reveal subunit arrangement and pore architecture. Nature 511, 191–197, doi:10.1038/nature13548 (2014). [PubMed: 25008524]
25. Gibb AJ et al. A structurally derived model of subunit-dependent NMDA receptor function. J Physiol 596, 4057–4089, doi:10.1113/JP276093 (2018). [PubMed: 29917241]
26. Ogden KK & Traynelis SF Contribution of the M1 transmembrane helix and pre-M1 region to positive allosteric modulation and gating of N-methyl-D-aspartate receptors. Mol Pharmacol 83, 1045–1056, doi:10.1124/mol.113.085209 (2013). [PubMed: 23455314]
27. Sobolevsky AI, Prodromou ML, Yelshansky MV & Wollmuth LP Subunit-specific contribution of pore-forming domains to NMDA receptor channel structure and gating. J Gen Physiol 129, 509–525, doi:10.1085/jgp.200609718 (2007). [PubMed: 17504910]

28. Kazi R et al. Asynchronous movements prior to pore opening in NMDA receptors. J Neurosci 33, 12052–12066, doi:10.1523/JNEUROSCI.5780-12.2013 (2013). [PubMed: 23864691]
29. Talukder I, Borker P & Wollmuth LP Specific sites within the ligand-binding domain and ion channel linkers modulate NMDA receptor gating. J Neurosci 30, 11792–11804, doi:10.1523/JNEUROSCI.5382-09.2010 (2010). [PubMed: 20810899]
30. Perszyk R et al. An NMDAR positive and negative allosteric modulator series share a binding site and are interconverted by methyl groups. Elife 7, doi:10.7554/eLife.34711 (2018).
31. Swanger SA et al. A Novel Negative Allosteric Modulator Selective for GluN2C/2D-Containing NMDA Receptors Inhibits Synaptic Transmission in Hippocampal Interneurons. ACS Chem Neurosci 9, 306–319, doi:10.1021/acschemneuro.7b00329 (2018). [PubMed: 29043770]
32. Zhu S et al. Mechanism of NMDA Receptor Inhibition and Activation. Cell 165, 704–714, doi:10.1016/j.cell.2016.03.028 (2016). [PubMed: 27062927]
33. Twomey EC & Sobolevsky AI Structural Mechanisms of Gating in Ionotropic Glutamate Receptors. Biochemistry 57, 267–276, doi:10.1021/acs.biochem.7b00891 (2018). [PubMed: 29037031]
34. Watanabe J, Beck C, Kuner T, Premkumar LS & Wollmuth LP DRPEER: a motif in the extracellular vestibule conferring high Ca2+ flux rates in NMDA receptor channels. Journal of Neuroscience 22, 10209–10216 (2002). [PubMed: 12451122]
35. Schewe M et al. A pharmacological master key mechanism that unlocks the selectivity filter gate in K+ channels. 363, 875–880, doi:10.1126/science.aav0569 %J Science (2019).
36. Traynelis SF & Jaramillo F Getting the most out of noise in the central nervous system. Trends Neurosci 21, 137–145 (1998). [PubMed: 9554720]
37. Lester RA, Clements JD, Westbrook GL & Jahr CE Channel kinetics determine the time course of NMDA receptor-mediated synaptic currents. Nature 346, 565–567, doi:10.1038/346565a0 (1990). [PubMed: 1974037]
38. Mizuta I, Katayama M, Watanabe M, Mishina M & Ishii K Developmental expression of NMDA receptor subunits and the emergence of glutamate neurotoxicity in primary cultures of murine cerebral cortical neurons. Cell Mol Life Sci 54, 721–725, doi:10.1007/s000180050199 (1998). [PubMed: 9711238]
39. Erreger K et al. Subunit-Specific Agonist Activity at NR2A-, NR2B-, NR2C-, and NR2D-Containing N-Methyl-D-aspartate Glutamate Receptors. Molecular Pharmacology 72, 907–920, doi:10.1124/mol.107.037333 (2007). [PubMed: 17622578]
40. Dravid SM, Prakash A & Traynelis SF Activation of recombinant NR1/NR2C NMDA receptors. J Physiol 586, 4425–4439, doi:10.1113/jphysiol.2008.158634 (2008). [PubMed: 18635641]
41. Wyllie DJ, Behe P, Nassar M, Schoepfer R & Colquhoun D Single-channel currents from recombinant NMDA NR1a/NR2D receptors expressed in Xenopus oocytes. Proceedings. Biological sciences / The Royal Society 263, 1079–1086, doi:10.1098/rspb.1996.0159 (1996).
42. Premkumar LS & Auerbach A Identification of a high affinity divalent cation binding site near the entrance of the NMDA receptor channel. Neuron 16, 869–880 (1996). [PubMed: 8608005]
43. Lewis CA Ion-concentration dependence of the reversal potential and the single channel conductance of ion channels at the frog neuromuscular junction. J Physiol 286, 417–445 (1979). [PubMed: 312319]
44. Jatzke C, Watanabe J & Wollmuth LP Voltage and concentration dependence of Ca(2+) permeability in recombinant glutamate receptor subtypes. J Physiol 538, 25–39 (2002). [PubMed: 11773314]
45. Siegler Retchless B, Gao W & Johnson JW A single GluN2 subunit residue controls NMDA receptor channel properties via intersubunit interaction. Nat Neurosci 15, 406–413, S401–402, doi:10.1038/nn.3025 (2012). [PubMed: 22246434]
46. Wollmuth LP & Sakmann B Different mechanisms of Ca2+ transport in NMDA and Ca2+-permeable AMPA glutamate receptor channels. J Gen Physiol 112, 623–636 (1998). [PubMed: 9806970]
47. Woodhull AM Ionic blockage of sodium channels in nerve. J Gen Physiol 61, 687–708 (1973). [PubMed: 4541078]

48. Rosenmund C, Stern-Bach Y & Stevens CF The tetrameric structure of a glutamate receptor channel. Science 280, 1596–1599 (1998). [PubMed: 9616121]

49. Zheng J & Sigworth FJ Selectivity Changes during Activation of Mutant Shaker Potassium Channels. The Journal of General Physiology 110, 101–117, doi:10.1085/jgp.110.2.101 (1997). [PubMed: 9236204]

50. Ikonomidou C & Turski L Why did NMDA receptor antagonists fail clinical trials for stroke and traumatic brain injury? Lancet Neurol 1, 383–386 (2002). [PubMed: 12849400]

References

51. Colquhoun D & Sigworth FJ in Single-Channel Recording (eds Bert Sakmann & Erwin Neher) 483–587 (Springer US, 1995).

52. Neher E Correction for liquid junction potentials in patch clamp experiments. Methods Enzymol 207, 123–131 (1992). [PubMed: 1528115]

53. Burnashev N, Zhou Z, Neher E & Sakmann B Fractional calcium currents through recombinant GluR channels of the NMDA, AMPA and kainate receptor subtypes. J Physiol 485 (Pt 2), 403–418 (1995). [PubMed: 7666365]

54. Paoletti P, Neyton J & Ascher P Glycine-independent and subunit-specific potentiation of NMDA responses by extracellular Mg2+. Neuron 15, 1109–1120 (1995). [PubMed: 7576654]

55. Traynelis SF Software-based correction of single compartment series resistance errors. Journal of Neuroscience Methods 86, 25–34, doi:10.1016/S0165-0270(98)00140-X (1998). [PubMed: 9894783]

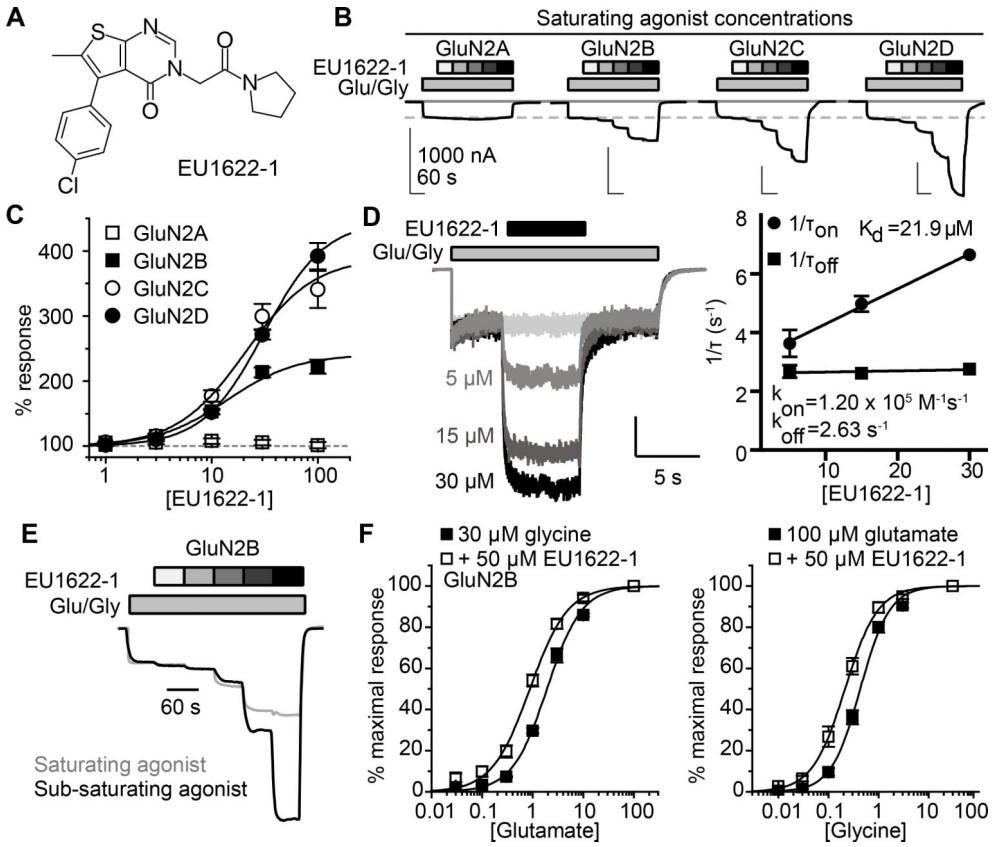

Figure 1.

EU1622-1 is a positive allosteric NMDAR modulator. (A) Structure of EU1622-1 (Compound **1**). (B) Two-electrode voltage-clamp oocyte recordings show effects of EU1622-1 (1,3,10,30,100 μM) co-applied with 100/30 μM glutamate/glycine. (C) Mean concentration-response data for EU1622-1 was fitted by the Hill equation. (D) EU1622-1 was co-applied with 100/30 μM glutamate and glycine onto GluN1/GluN2B-expressing HEK cells by rapid-solution exchange. The onset of EU1622-1 potentiation was fitted with an exponential function, and τ_{on} (1/time constant) plotted *vs.* EU1622-1 concentration. The association rate k_{on} was the slope and the *y* intercept was the dissociation constant, k_{off} (n = 7 cells); K_D was the ratio of k_{off}/k_{on}. (E) EU1622-1 concentration-response curve in sub-saturating (1.5/0.45 μM) glutamate/glycine at GluN1/GluN2B in oocytes; The GluN1/GluN2B response from (A) is shown again in gray. (F) Glutamate (*left*) and glycine (*right*) mean concentration-response data from GluN1/GluN2B expressed in oocytes in the absence and presence of 50 μM EU1622-1, fitted by the Hill equation.

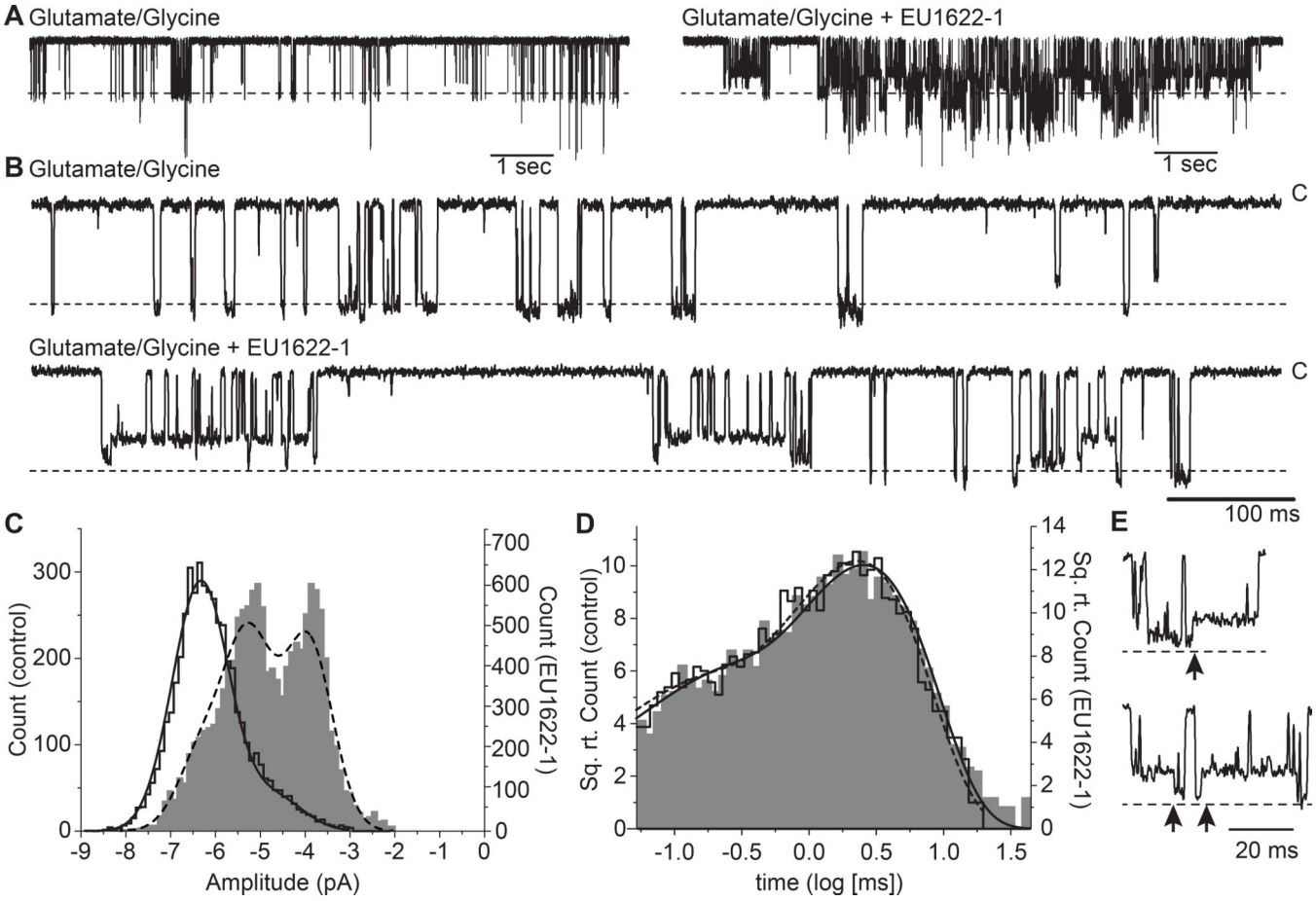

Figure 2.

EU1622-1 reduces single channel conductance for GluN1/GluN2B NMDARs. (A) Unitary currents were recorded from an outside-out patch excised from an HEK cell co-transfected with GluN1, GluN2B, and GFP. The holding potential was −80 mV and channel openings are shown as downward by convention. Responses were produced by the application of external solution with 0.1 mM glutamate plus 0.05 mM glycine (0.5 mM Ca^{2+}). NMDARs showed reduced unitary current amplitude when 50 μM EU1622-1 was co-applied with the agonist (*lower panel*) compared to vehicle (*upper panel*). (C) Composite amplitude histograms determined by time course fitting were analyzed by fitting with the sum of multiple Gaussian components by maximum likelihood for vehicle (open bars, solid line, left y-axis) and 30–50 μM EU1622-1 (filled bars, dashed line, right y-axis). Supplementary Table 8 provides a summary of chord conductance. (D) Composite open duration histograms for the patch shown and fitted by the sum of two exponential components displayed similarly to (C). Mean open time is given in Supplementary Table 8; individual fitted time constants ± standard deviation and area for the fits were: vehicle Tau_1 0.10 ± 0.0028 ms, 12%, Tau_2 2.3 ± 0.31 ms, 88%, EU1622-1 Tau_1 0.54 ± 0.40 ms, 26%, Tau_2 3.2 ± 0.93 ms, 74% (n = 3 patches). (E) Examples of direct sublevel transitions in the presence of EU1622-1 are shown, marked by arrowheads.

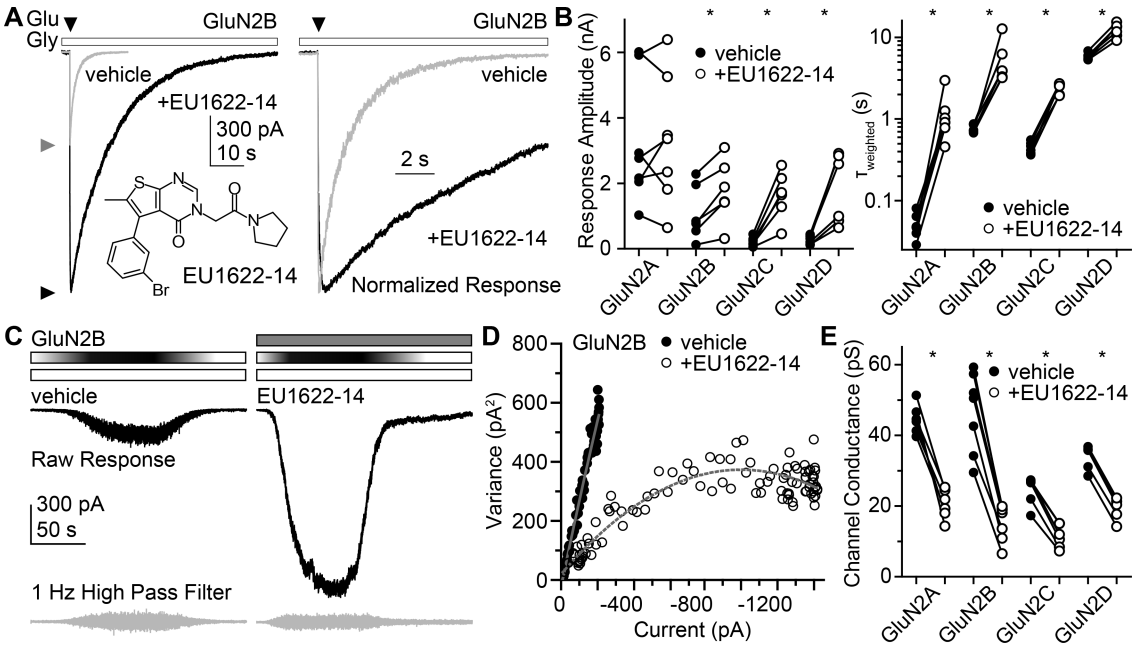

Figure 3.

EU1622-14 prolongs the response deactivation time course and reduces channel conductance of NMDARs. (A) Representative GluN1/GluN2B NMDAR current responses during rapid application of 1/0.1 mM glutamate/glycine for 10 ms (triangle) in 100 μM glycine (white bar) with vehicle or EU1622-14 (30 μM, Compound **2**). Horizontal triangles show peak amplitudes. An expanded, normalized view is shown on the right to highlight the deactivation time course of the responses. (B) Peak amplitude (*left*) and $\tau_{weighted}$ of the deactivation (*right*) of rapid glutamate applications (10 ms) with and without EU1622-14 for all diheteromeric NMDARs (see Supplementary Table 4). (C) Representative slow perfusion stimulated GluN1/GluN2B responses with glutamate and glycine co-applied with vehicle or E1622-14. The NMDAR-mediated increase in variance can be seen from the high-pass filtered current (grey, below). (D) Current-variance plot of the rise and decay of the low concentration agonist application from (C). (E) Mean conductance of all diheterometic NMDARs with and without EU1622-14 (50 μM). For summary data see Supplementary Table 4. For all panels, * $p<0.05$ by paired t-test, with the Holm-Bonferroni correction to control for the family wise error rate in (B).

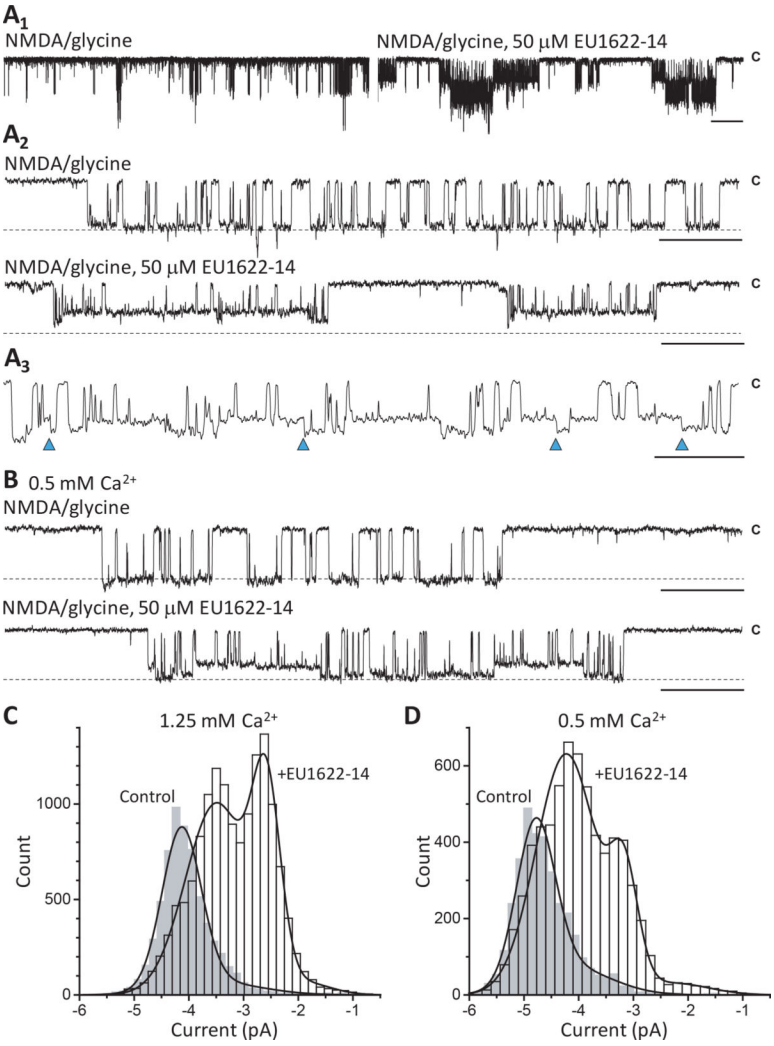

Figure 4.

EU1622-14 reduces native NMDAR conductance. Unitary currents activated by 500 μM NMDA and 100 μM glycine (−80 mV) in outside-out patches were from cortical neurons in 1.25 (A) or 0.5 mM Ca^{2+} (B); scale bars are 2 s (A_1), 100 ms (A_2) and 50 ms (A_3). The dashed line is 5 pA. "C" indicates closed state and arrowheads in A_3 show sublevel transitions in EU1622-14. Vehicle was 0.25% DMSO. (C,D) Amplitudes determined (6,369 vehicle, 14,406 EU1622-14) from 6 patches in 1.25 mM Ca^{2+} or 4 patches (3,473 vehicle, 6,639 EU1622-14) in 0.5 mM Ca^{2+} were fitted to the sum of 2–3 Gaussians (smooth line is the probability density function). The amplitude ± standard deviation and area for the fits (1.25 mM Ca^{2+}) were: vehicle Amp_1 −4.13 ± 0.36 pA, 85%, Amp_2 −3.52 ± 0.83 pA, 15%, EU1622-14 Amp_1 −3.45 ± 0.59 pA, 71% Amp_2 −2.58 ± 0.22 pA, 23% Amp_3 −2.16 ± 0.57 pA, 6 %. The amplitude ± standard deviation and area for the fits (0.5 mM Ca^{2+}) were: vehicle Amp_1 −4.79 ± 0.35 pA, 73% Amp_2 −4.16 ± 0.75 pA, 27%, EU1622-14 Amp_1 −4.23 ± 0.55 pA, 79%, Amp_2 −3.17 ± 0.26 pA, 16% Amp_3 −2.27 ± 0.65 pA, 4%.

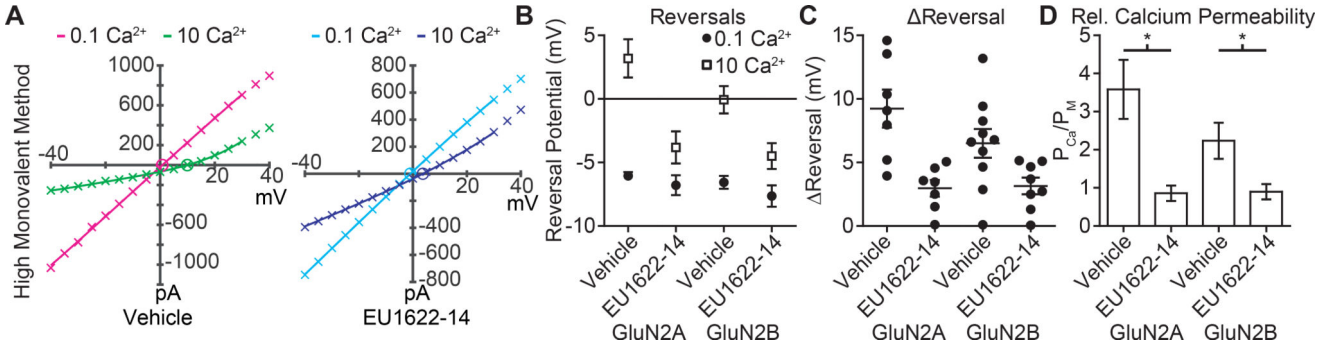

Figure 5.

EU1622-14 reduces Ca^{2+} permeation through NMDARs. (A) Representative I-V curves for GluN1/GluN2A responses to maximally-effective agonist co-applied with vehicle (*left*) or EU1622-14 (*right*) in the low/high Ca^{2+}. A high monovalent method was used to determine the relative Ca^{2+}/monovalent permeability ratio. The fitted curve is a fourth-order polynomial. (B) The average reversal potentials are given for GluN1/GluN2A and GluN1/GluN2B (vehicle vs. EU1622-14). (C) The mean ΔReversal potentials (high Ca^{2+} minus low Ca^{2+}) are given. (D) The average Ca^{2+} permeability ratio to monovalent ions is from the Lewis equation. *p<0.05 (One-way ANOVA, post-hoc t-test of drug *vs* vehicle, Bonferroni correction for multiple comparisons); $F_{3,28} = 6.91$. For summary data see Supplementary Table 9.

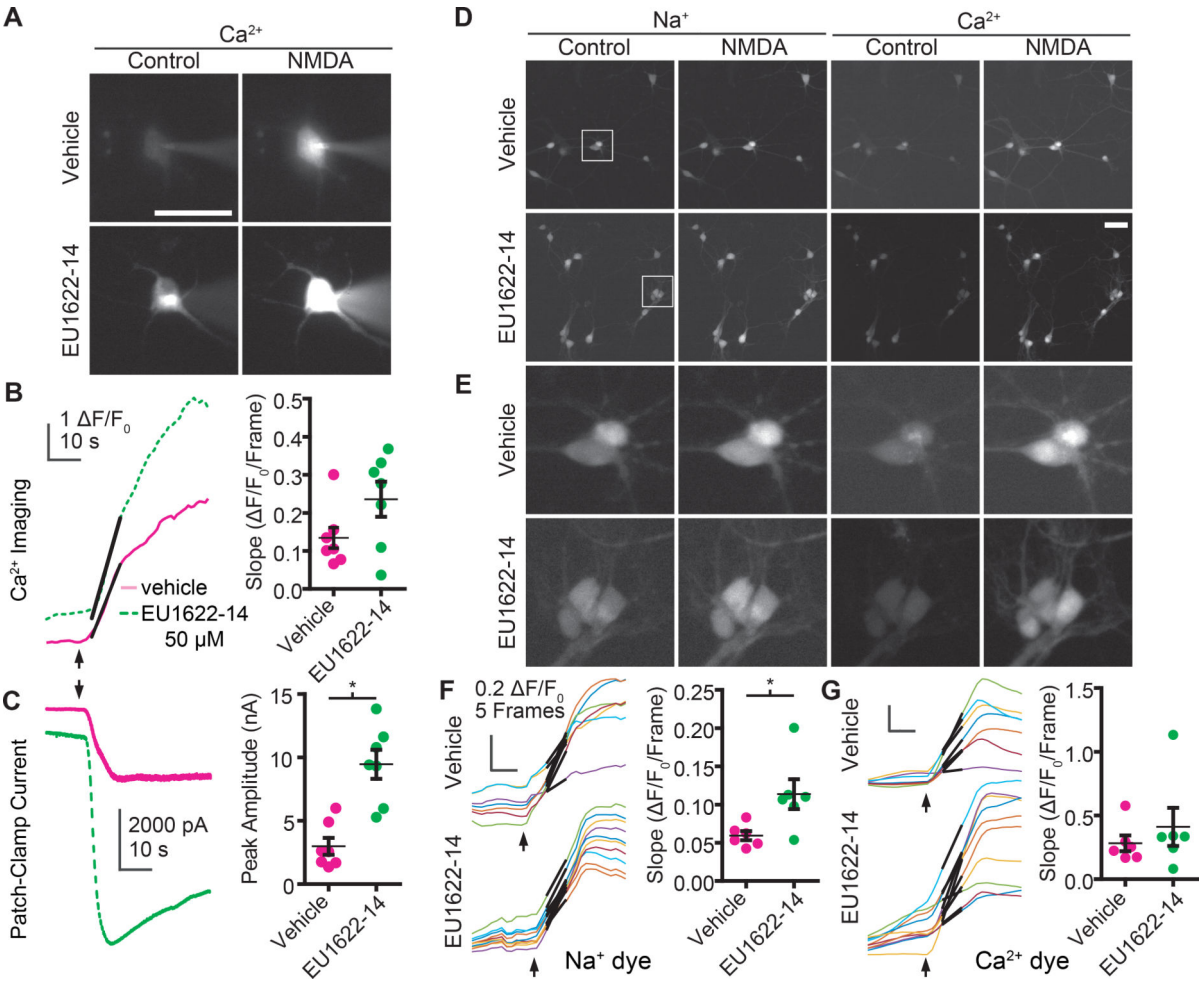

Figure 6.

EU1622-14 biasedly modulates Na^+ and Ca^{2+} influx through NMDARs. (A-C) Simultaneous patch-clamp/imaging recordings from cortical neuronal cultures illustrate a significant augmentation of total current with a non-significant increase in the Ca^{2+} fluorescence (stimulated by 500/100 μM NMDA/glycine) due to EU1622-14 modulation. (A) Time-lapse imaging of a Ca^{2+}-sensitive, cell impermeant dye (Calbryte 590 potassium-salt, images were taken at a 1s interval). Representative vehicle and EU1622-14 fluorescence B, *left*) and current (C, *left*) responses to 500/100 μM NMDA/glycine co-applied with vehicle (equivalent volume DMSO) or EU1622-14 (50 μM) following a 1 min pre-application of vehicle or drug. Summary graphs are shown on the *right* of each figure panel. A significant increase in the peak current amplitude ($p = 0.0004$, unpaired t-test) was detected in the presence of EU1622-14 (50 μM) but not a significant increase in the slope of the Ca^{2+}-fluorescence signal ($p = 0.09$, unpaired t-test). (D-G) Simultaneous fluorescence monitoring of Na^+ and Ca^{2+} influx using specific cell permeable dyes illustrates selective modulation by EU1622-14. (D) Intracellular Na^+ and Ca^{2+} levels were measured in cortical neuronal cultures utilizing time-lapse imaging of Na^+- and Ca^{2+}-sensitive dyes. 500/100 μM NMDA/glycine were co-applied in vehicle (0.5% DMSO) or EU1622-14 (50 μM) following a 1 min pre-application of vehicle or drug. Images were acquired every 4 s. Boxed regions in

(E) are shown in (D). (F-G) Cellular fluorescence responses to NMDAR stimulation in the presence of vehicle or EU1622-14. Agonist solution perfusion (indicate by the arrow, 500/100 μM NMDA/glycine, with vehicle or EU1622-14) resulted in a rise in the CoroNa AM dye (F, Na^+ response) and the Calbryte 590 AM dye (G, Ca^{2+} response). For each trial, the slope of the rise of the respective signals were measured for all neurons in the camera view, then averaged to obtain one experimental data point (shown in the plot on the *right*). Scale bars denote 50 μm.